TROSY in triple-resonance experiments: New perspectives for sequential NMR assignment of large proteins

MICHAEL SALZMANN*†, KONSTANTIN PERVUSHIN*, GERHARD WIDER*, HANS SENN†, AND KURT WÜTHRICH*‡

*Institut für Molekularbiologie und Biophysik, Eidgenössische Technische Hochschule Hönggerberg, CH-8093 Zürich, Switzerland; and †F. Hoffmann-La Roche AG, Pharma Research, CH-4070 Basel, Switzerland

Contributed by Kurt Wüthrich, September 10, 1998

ABSTRACT The NMR assignment of ^{13}C, ^{15}N-labeled proteins with the use of triple resonance experiments is limited to molecular weights below $\sim$25,000 Daltons, mainly because of low sensitivity due to rapid transverse nuclear spin relaxation during the evolution and recording periods. For experiments that exclusively correlate the amide proton (^{1}H^N), the amide nitrogen (^{15}N), and ^{13}C atoms, this size limit has been previously extended by additional labeling with deuterium (^{2}H). The present paper shows that the implementation of transverse relaxation-optimized spectroscopy ([^{15}N,^{1}H]-TROSY) into triple resonance experiments results in several-fold improved sensitivity for ^{2}H/^{13}C/^{15}N-labeled proteins and approximately twofold sensitivity gain for ^{13}C/^{15}N-labeled proteins. Pulse schemes and spectra recorded with deuterated and protonated proteins are presented for the [^{15}N, ^{1}H]-TROSY-HNCA and [^{15}N, ^{1}H]-TROSY-HNCO experiments. A theoretical analysis of the HNCA experiment shows that the primary TROSY effect is on the transverse relaxation of ^{15}N, which is only little affected by deuteration, and predicts sensitivity enhancements that are in close agreement with the experimental data.

In the standard protocol for protein structure determination by NMR spectroscopy, sequence-specific resonance assignment plays a pivotal role (1). Several different assignment strategies are available, and one of the established procedures for obtaining sequential assignments (2) involves uniform ^{13}C/^{15}N labeling and delineation of heteronuclear scalar couplings with triple-resonance experiments (3–7). In these experiments, the transfer of magnetization along networks of scalar-coupled spins includes long delays during which ^{13}C and ^{15}N magnetization evolve in the transverse plane. Fast transverse relaxation during these delays and during ^{1}H acquisition, limits the application of triple-resonance NMR experiments with larger proteins. For experiments that exclusively correlate ^{1}H^N, ^{15}N, and ^{13}C, the situation has been improved by ^{2}H-labeling of the ^{13}CH$_n$ moieties, which eliminates dipolar ^{13}C relaxation by the directly attached protons (8) and reduces ^{1}H^N line broadening by dipole–dipole (DD) coupling with remote protons. However, uniform deuteration also imposes stringent limitations on the structural information that can be obtained by NMR (8,9) and does not significantly reduce ^{15}N relaxation during the delays when this spin is in the transverse plane. Here, we propose to extend the application of triple-resonance experiments by using the principle of transverse relaxation-optimized spectroscopy (TROSY) (10). TROSY suppresses transverse relaxation in ^{15}N–^{1}H^N moieties by constructive use of interference between dipole–dipole coupling and chemical shift anisotropy (CSA) (10) and thus results in improved sensitivity of triple-resonance experiments by minimizing ^{15}N transverse relaxation during ^{15}N evolution periods and ^{1}H^N transverse relaxation during detection. Because part of the gain achieved

with TROSY stems from the reduced T$_2$ relaxation rate of ^{15}N, TROSY will benefit triple-resonance experiments with deuterated as well as protonated proteins. In this paper, we present experimental schemes for the implementation of TROSY in the amide proton-to-nitrogen-to-α carbon correlation (HNCA) and amide proton-to-nitrogen-to-carbonyl carbon correlation (HNCO) experiments, which correlate the ^{15}N–^{1}H(i) group with ^{13}C$^\alpha$(i) and ^{13}C$^\alpha$($i-1$), and with ^{13}CO($i-1$), respectively (11, 12). For a quantitative evaluation of the sensitivity gain that can be achieved, we compare [^{15}N, ^{1}H]-TROSY-HNCA with conventional HNCA (13).

METHODS

Triple-resonance experiments use coherence transfers along a network of scalar coupled ^{15}N, ^{13}C, and ^{1}H spins (3–7). Thereby, coherence transfer from ^{15}N to either ^{13}C$^\alpha$ or ^{13}CO requires long delays due to the small ^{1}J(^{15}N, ^{13}C$^\alpha$)- and ^{1}J(^{15}N, ^{13}CO)-coupling constants. Because the ^{15}N magnetization is in the transverse plane throughout these transfer periods, the ^{15}N chemical shift evolution is recorded in a constant-time (ct) fashion during the magnetization transfer (14, 15), and relaxation of ^{15}N due to DD coupling with the directly bound ^{1}H^N and to ^{15}N CSA leads to severe loss of coherence. Using the TROSY principle (10), transverse relaxation during these critical ^{15}N evolution periods can be efficiently suppressed. Similarly, ^{1}H^N transverse relaxation during detection due to ^{1}H^N CSA and to DD coupling with ^{15}N can be suppressed with the use of TROSY.

In the following product operator analysis (16) of the [^{15}N, ^{1}H]-TROSY-HNCA experiment (Fig. 1), we describe the ^{13}C magnetization (C) with Cartesian operators, whereas for the ^{1}H^N (H) and ^{15}N (N) magnetizations single-transition operators (17) are used. For both ^{13}C/^{15}N- and ^{2}H/^{13}C/^{15}N-labeled proteins, the ^{1}H as well as the ^{15}N steady–state magnetizations are used at the outset, and the density matrix after the first insensitive nuclei enhanced by polarization transfer (INEPT) step at time point b in Fig. 1 becomes

$$\sigma_b = i\,\frac{(u+v)}{2}\,(N_r^- - N_r^+) - i\,\frac{(u-v)}{2}\,(N_s^- - N_s^+), \quad [1]$$

where the constant factors u and v represent the relative magnitudes of the steady–state ^{1}H and ^{15}N magnetizations (18, 19), and the single-transition operators $N_r^\pm$ and $N_s^\pm$ represent the ^{15}N magnetization associated with the rotating frame transition frequencies $\omega_s^N = \omega^N + \pi J_{HN}$ and $\omega_r^N = \omega^N - \pi J_{HN}$, respectively (20). Only the N_s^- and N_s^+ terms are transferred to detectable magnetization after the single transition-to-single transition polarization transfer (ST2-PT) element (18) (time points e–f in Fig. 1). During the ct period $T/2$ between time points b and c, the $N_s^\pm$ spin operators evolve due to the ^{15}N chemical shift and the J-couplings

Abbreviations: ct, constant-time; DD, dipole–dipole; CSA, chemical shift anisotropy; HNCA, amide proton-to-nitrogen-to-α carbon correlation; HNCO, amide proton-to-nitrogen-to-carbonyl carbon correlation; ST2-PT, single transition-to-single transition polarization transfer; TROSY, transverse relaxation-optimized spectroscopy; 3D, three-dimensional.
‡To whom reprint requests should be addressed,

to the two neighboring α-carbons, $^{13}C^{\alpha}(i)$ and $^{13}C^{\alpha}(i-1)$. The resulting antiphase terms $N_s^{\pm} C_z^{\alpha}(i)$ and $N_s^{\pm} C_z^{\alpha}(i-1)$ are converted to multiple-quantum coherences by the 90° ($^{13}C^{\alpha}$) pulse at time point c. During t_2, these terms evolve due to the $^{13}C^{\alpha}$ chemical shift because carbonyl carbons and deuterons or protons are decoupled (Fig. 1). The 90° ($^{13}C^{\alpha}$) pulse at time point d completes the $^{13}C^{\alpha}$ evolution period. During the second half of the ct ^{15}N evolution period, the $N_s^{\pm} C_z^{\alpha}(i)$ and $N_s^{\pm} C_z^{\alpha}(i-1)$ terms again evolve due to the ^{15}N chemical shift (21),

$$\sigma_e = i \frac{(u-v)}{2} N_s^{\pm}(T)[cos(\omega^C(i)t_2) + cos(\omega^C(i-1)t_2)]. \quad [2]$$

Two signals in the $^{13}C(t_2)$ dimension exhibit the intraresidual correlation $\omega_1(^{15}N_i)/\omega_2(^{13}C_i^{\alpha})$ modulated by $cos(\omega^C(i)t_2)$ and the sequential correlation $\omega_1(^{15}N_i)/\omega_2(^{13}C_{i-1}^{\alpha})$ modulated by $cos(\omega^C(i-1)t_2)$. Transverse ^{15}N relaxation during the ct period $T = 1/^1J_{NC^{\alpha}}$ is given by (see *Appendix*):

$$N_s^{\pm}(T) = N_s^{\pm}(0) \cdot exp(\mp i\omega_s^N t_1) \cdot exp[-R_s^N T]$$

$$\cdot \prod_{j=1}^{n} 0.5(1 + exp[-2p_{HK^j}^2 J(0)T]), \quad [3]$$

where the term $p_{HK^j}^2 J(0)$ represents the relaxation of ^{15}N due to DD interactions of $^1H^N$ (H) with remote protons K^j (see *Appendix*) and R_s^N is the ^{15}N relaxation rate due to DD coupling with $^1H^N$ and to ^{15}N chemical shift anisotropy CSA. Auto- and cross-relaxation terms due to $^{13}C^{\alpha}$–^{15}N and ^{13}CO–^{15}N DD coupling were neglected because they contribute <10% to the overall relaxation rate of ^{15}N (see *Appendix*). The ST2-PT element (18) (Fig. 1, e-f) transfers the magnetization from ^{15}N to $^1H^N$ ($N_s^+ \rightarrow H_s^-$), resulting in the following coherence being acquired during t_3:

$$\sigma_{rec} = i \frac{(u-v)}{2} H_s^-(t_3) \cdot \left[exp(-i\omega_s^N t_1) \cdot exp[-R_s^N T] \right.$$

$$\cdot \prod_{j=1}^{n} 0.5(1 + exp[-2p_{HK^j}^2 J(0)T]) \bigg]$$

$$\cdot [cos(\omega^C(i)t_2) + cos(\omega^C(i-1)t_2)] \quad [4]$$

In Eq. 4, the transition H_s^- is associated with the resonance frequency $\omega_s^H = \omega^H + \pi J_{HN}$, and the $^1H^N$ relaxation is given by Eq. 5 (10):

$$H_s^-(t_3) = H_s^-(0) \cdot exp(+i\omega_s^H t_3) \cdot exp[-R_s^H t_3]$$

$$\cdot \prod_{j=1}^{n} exp[-5p_{HK^j}^2 J(0)t_3], \quad [5]$$

where R_s^H is the $^1H^N$ relaxation rate due to DD coupling with ^{15}N and to $^1H^N$ CSA (10).

EXPERIMENTAL PROCEDURES

NMR spectra were recorded with two 23-kDa globular proteins, i.e., uniformly $^2H/^{13}C/^{15}N$-labeled gyrase-23B (95% H_2O/5% D_2O, pH 6.5 at 20°C) (22–24) and uniformly $^{13}C/^{15}N$-labeled FimC (90% H_2O/10% D_2O, pH 5.0 at 20°C) (25). A Bruker DRX-750 spectrometer equipped with four radio-frequency channels was used. Data processing included zero-filling and sine bell filtering (26), using the program PROSA (27), and the spectra were analyzed with XEASY (28). For gyrase-23B and FimC at 20°C, the isotropic rotational correlation time, τ_c, was estimated from the T_1/T_2 ratio of the backbone ^{15}N nuclei (29) to be 15 ns.

RESULTS

The pulse sequence of Fig. 1 was applied with $^2H/^{13}C/^{15}N$-labeled gyrase-23B (22–24) and $^{13}C/^{15}N$-labeled FimC (25). Fig. 2a shows $[\omega_2(^{13}C), \omega_3(^1H)]$ strips from a three-dimensional (3D) $[^{15}N, ^1H]$-TROSY-HNCA spectrum of gyrase-23B, and Fig. 2b
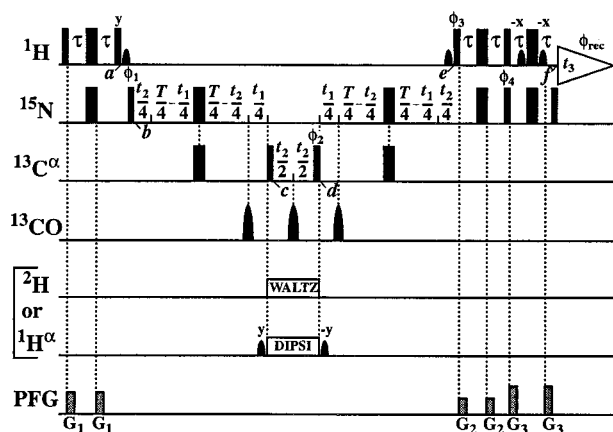
FIG. 1.   Experimental scheme for the $[^{15}N, ^1H]$-TROSY-HNCA experiment. The radio-frequency pulses on ^1H, ^{15}N, $^{13}C^{\alpha}$, ^{13}CO, ^2H, and $^1H^{\alpha}$ are applied at 4.7, 118, 56, 177, 3.6, and 4.7 ppm, respectively. Narrow and wide black bars indicate nonselective 90° and 180° pulses. Sine bell shapes on the lines marked ^1H and $^1H^{\alpha}$ indicate selective 90° pulses. On the line marked ^{13}CO, three selective 180° pulses are applied off-resonance with a duration of 120 μs and a Gaussian shape. The line marked PFG indicates the durations and amplitudes of pulsed magnetic field gradients applied along the z-axis: G_1: 800 μs, 15 G/cm; G_2: 800 μs, 9 G/cm; and G_3: 800 μs, 22 G/cm. The delays are $\tau = 2.7$ ms and $T = 44$ ms. The phase cycle is: $\phi_1 = \{y, -y, -x, x\}$; $\phi_2 = \{4x, 4(-x)\}$; $\phi_3 = \{-y\}$; $\phi_4 = \{-y\}$; $\phi_{rec} = \{y, -y, -x, x, -y, y, x, -x\}$, with all other radio-frequency pulses applied with phase x. A phase-sensitive spectrum in the $^{15}N(t_1)$ dimension is obtained by recording a second FID for each t_1 value, with $\phi_1 = \{y, -y, x, -x\}$, $\phi_3 = \{y\}$ and $\phi_4 = \{y\}$, and data processing as described by Kay *et al.* (41). Quadrature detection in the $^{13}C^{\alpha}(t_2)$ dimension is achieved by the States-TPPI method (42) applied to the phase ϕ_2. The use of water flip-back pulses (43) at times a and e ensures that the water magnetization stays aligned along +z throughout both the ct period T and the data acquisition period t_3. Residual transverse water magnetization is suppressed immediately before data acquisition (44). The scheme is used for two alternative experiments. For ^2H-labeled proteins, ^2H-decoupling during t_2 is achieved with WALTZ-16 composite pulse decoupling (45) at a field strength of $\gamma B_2 = 2.5$ kHz. For measurements with protonated proteins, selective $^1H^{\alpha}$-decoupling during the $^{13}C^{\alpha}(t_2)$ evolution period is applied instead, using a DIPSI-2 decoupling scheme (46) with $\gamma B_2 = 0.51$ kHz. The two selective pulses on the water resonance before and after DIPSI-2 ensure the correct treatment of the water during the subsequent t_1 and t_2 evolution periods.

shows the corresponding strips from a conventional HNCA experiment (13) recorded with identical conditions. Using TROSY, all sequential $^1H^N$-$^{13}C^{\alpha}$ connectivities could be identified, as indicated by the broken lines (Fig. 2a), whereas with conventional HNCA no reliable sequential assignment was possible (Fig. 2b). A more quantitative assessment of the gain in signal-to-noise is afforded by the cross sections in Fig. 2a' and b'. Data of this type were collected in Fig. 3 for the complete sequence of gyrase-23B. In $[^{15}N, ^1H]$-TROSY-HNCA (Fig. 3a), nearly all sequential cross peaks were present with sufficient intensity to allow sequential assignments, which was feasible only for a fraction of the sequence when conventional HNCA is used (Fig. 3b). TROSY also yielded greatly increased intensities of the intraresidual correlation peaks $[\omega_1(^{15}N_i)/\omega_2(^{13}C_i^{\alpha})/\omega_3(^1H_i^N)]$ (Fig. 3a' and b'). In line with theoretical considerations (10), the highest sensitivity gains were obtained for the immobilized core of the protein, with values of 2.9 for the α-helices and 3.4 for the β-sheets. The average sensitivity gain for sequential and intraresidual correlation peaks of the entire protein was 2.4-fold.

Measurements corresponding to those in Figs. 2 and 3 also were performed with uniformly $^{13}C/^{15}N$-labeled FimC in order to evaluate the performance of $[^{15}N, ^1H]$-TROSY-HNCA with protonated proteins. The experimental scheme of Fig. 1 was used with $^1H^{\alpha}$ decoupling. The average sensitivity enhancement for the
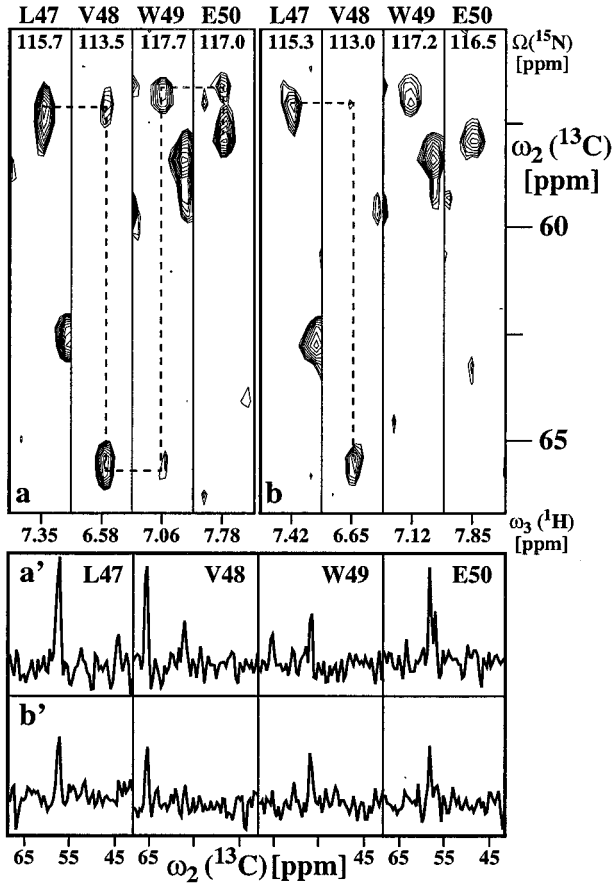
FIG. 2. Comparison of *a* [^{15}N, ^{1}H]-TROSY-HNCA recorded with the scheme of Fig. 1 and *b* conventional HNCA (13) using ^{1}H DIPSI-2 decoupling with $\gamma B_2 = 3.13$ kHz during t_1 and t_2, and ^{15}N WALTZ-16 decoupling with $\gamma B_2 = 1.6$ kHz during acquisition. Both experiments were recorded with a 1 mM solution of uniformly ^{2}H/^{13}C/^{15}N-labeled gyrase-23B. $26(t_1) \times 32(t_2) \times 512(t_3)$ complex points were accumulated, with $t_{1max}(^{15}$N$) = 21.7$, $t_{2max}(^{13}$C$^\alpha) = 6.4$, and $t_{3max}(^1$H$) = 48.7$ ms. Fifty-six scans per increment were acquired, resulting in a total measuring time of 38 h per 3D spectrum. Corresponding [$\omega_2(^{13}$C$),\omega_3(^1$H$)$] strips from the two 3D experiments centered about the ^{1}H^N chemical shifts were taken at the ^{15}N chemical shifts of residues 47–50. Because no decoupling during t_1 and t_3 is used in TROSY, the amide ^{1}H^N and ^{15}N resonances in *a* are shifted in both dimensions by ≈ 45 Hz relative to the corresponding resonances in *b*. The sequence-specific assignments are indicated at the top by the one-letter amino acid symbol and the residue number in the amino acid sequence. In both spectra, dashed lines indicate sequential connectivities that could be reliably identified (see text). (*a'* and *b'*) cross sections along the $\omega_2(^{13}$C$)$ dimension through the four [$\omega_2(^{13}$C$),\omega_3(^1$H$)$] strips at the $\omega_3(^1$H$)$ positions indicated at the bottom in *a* and *b*, respectively, where the complete chemical shift range acquired in the $\omega_2(^{13}$C$)$ dimension is plotted.

entire protein was 1.5-fold, with a sensitivity gain of 1.7 for the regular secondary structures, which in FimC consist exclusively of β-sheets.

The pulse scheme of the [^{15}N, ^{1}H]-TROSY-HNCO experiment (Fig. 4*a*) was applied to ^{2}H/^{13}C/^{15}N-labeled gyrase-23B with identical conditions to those described for the HNCA experiment in Fig. 2. As an illustration of the results obtained, Fig. 4*b* and *c* compares corresponding cross-sections from [^{15}N, ^{1}H]-TROSY-HNCO and conventional HNCO (30). From a corresponding data set to Fig. 3, the average gain in sensitivity for the entire protein was found to be 2.4-fold, with values of 2.5 and 2.9 for the α-helices and the β-sheets, respectively.

DISCUSSION

The HNCA and HNCO measurements (Figs. 2–4) showed that significant improvement of triple resonance experiments can be
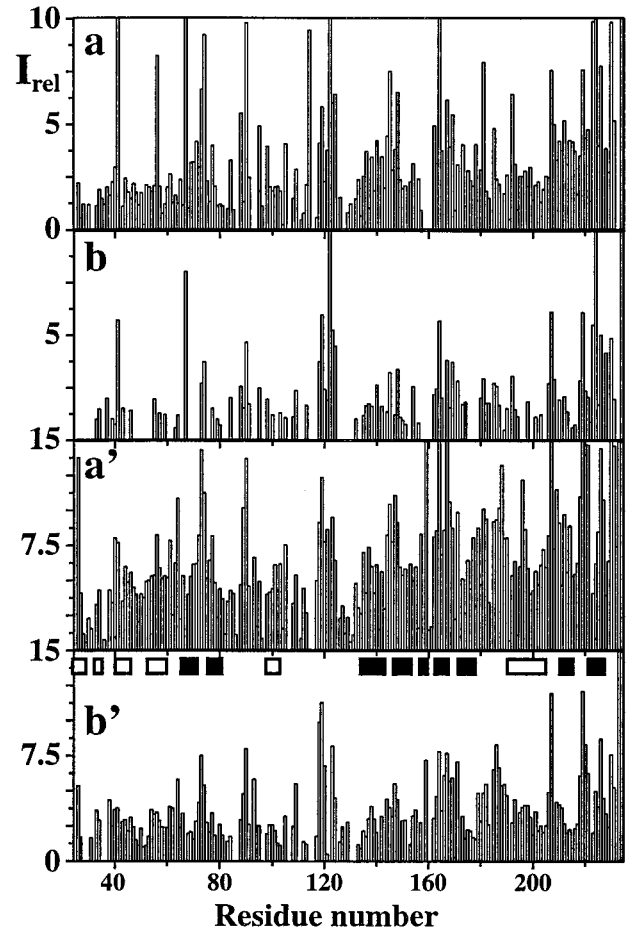
FIG. 3. Plots of the relative signal intensities, I_{rel}, along the amino acid sequence of uniformly ^{2}H/^{13}C/^{15}N-labeled gyrase-23B (1 mM protein concentration in 95% H$_2$O/5% D$_2$O at pH 6.5 and T = 20°C). (*a*) Sequential correlation peaks ($\omega_2(^{13}$C$^\alpha_{i-1})/\omega_3(^1H^N_i)$) in [^{15}N, ^{1}H]-TROSY-HNCA. (*b*) Same as *a* measured with conventional HNCA (13). (*a'*) Intraresidual correlation peaks ($\omega_2(^{13}$C$^\alpha_i)/\omega_3(^1$H$^N_i)$) in [^{15}N, ^{1}H]-TROSY-HNCA. (*b'*) Same as *a'* measured with conventional HNCA. Both spectra were recorded with the same experimental conditions and processed identically, as described in the text. The α-helical and β-sheet regions in the x-ray structure of gyrase-23B (22) are identified in *b'* by open and filled bars, respectively.

achieved by suppression of transverse ^{15}N and ^{1}H^N relaxation with TROSY. In this section, the origins of the enhanced sensitivity of [^{15}N, ^{1}H]-TROSY-HNCA are further analyzed.

In Eq. **5**, the ^{1}H^N relaxation can be represented by a single exponential, with the rate constant

$$R_2^T(^1\text{H}^\text{N}) \equiv \frac{1}{t_3} ln(exp[-R_s^H t_3] \cdot \prod_{j=1}^{n} exp[-5p_{HKj}^2 J(0)t_3])$$

$$= R_s^H + \sum_{j=1}^{n} 5p_{HKj}^2 J(0), \qquad [6]$$

where $R_2^T(^1$H$^N)$ denotes the transverse ^{1}H^N relaxation rate in [^{15}N, ^{1}H]-TROSY-HNCA. To a good approximation for the molecular size range of interest, the ^{15}N relaxation in [^{15}N, ^{1}H]-TROSY-HNCA (Eq. **3**) may similarly be represented by a single exponential decay, with the rate constant $R_2^T(^{15}$N$)$:

$$R_2^T(^{15}\text{N}) \equiv \frac{1}{T} ln(exp[-R_s^N T] \prod_{j=1}^{n} 0.5(1 + exp[-2p_{HKj}^2 J(0)T]))$$

$$\approx R_s^N + \sum_{j=1}^{n} p_{HKj}^2 J(0). \qquad [7]$$
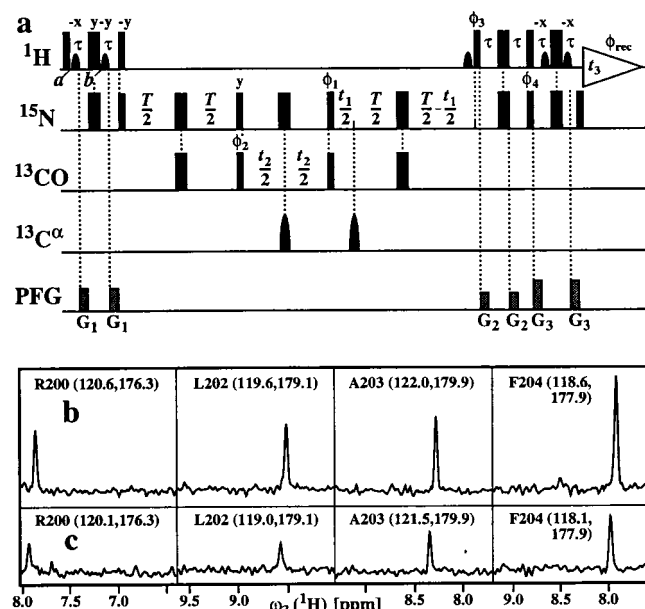
FIG. 4. (*a*) Experimental scheme for the [^{15}N, ^{1}H]-TROSY-HNCO experiment. All experimental parameters and the phase cycle are the same as in the [^{15}N, ^{1}H]-TROSY-HNCA scheme of Fig. 1. (*b* and *c*) Show, respectively, cross sections along the $\omega_3(^1$H) dimension through four peaks of the 3D [^{15}N, ^{1}H]-TROSY-HNCO spectrum and the conventional 3D HNCO spectrum (30) of uniformly ^{2}H/^{13}C/^{15}N-labeled gyrase-23B (1 mM protein concentration in 95% H$_2$O/5% D$_2$O at pH 6.5 and T = 20°C). 26(t_1) × 30(t_2) × 512(t_3) complex points were accumulated, with t_{1max} (^{15}N) = 10.8, t_{2max}(^{13}CO) = 12.0, and t_{3max}(^{1}H) = 48.7 ms. Eight scans per increment were acquired, resulting in a total measuring time of 7 h per 3D spectrum. At the top of each panel, the sequence-specific assignment is indicated by the one-letter amino acid symbol and the residue number in the amino acid sequence, and the $\omega_1(^{15}$N) and $\omega_2(^{13}$CO) chemical shifts are indicated in parentheses.

The approximation of Eq. **7** assumes that $p^2_{HK^j}J(0)T \ll 1$, which is satisfied for commonly used ct periods, T, over the τ_c range 1–80 ns. For the conventional HNCA experiment, corresponding transverse relaxation rates, $R_2^C(^{15}$N) and $R_2^C(^1$H^N), were evaluated as the average of the relaxation rates in the individual components of the ^{15}N and ^{1}H^N doublets, respectively. Using Eqs. **6** and **7** for a 23-kDa protein with τ_c = 15 ns at 750 MHz, and the

corresponding formalism for conventional HNCA, one predicts for the protonated protein that TROSY yields 2.9-fold and 1.5-fold reductions of the ^{15}N and ^{1}H^N relaxation rates, respectively, when compared to conventional HNCA (Table 1). For conventional HNCA, one expects further that deuteration reduces the ^{1}H^N relaxation rates 2.5-fold and 1.6-fold for β-sheets and α-helices, respectively, and that deuteration yields only a small reduction, by less than a factor 1.3, of the ^{15}N relaxation rate. For [^{15}N, ^{1}H]-TROSY-HNCA, deuteration has approximately the same absolute effects on $R_2^T(^{15}$N) and $R_2^T(^1$H^N), but because of the greatly reduced R_s^N and R_s^H rates the relative improvement is larger, i.e., up to 6.5 for ^{1}H^N and up to 2.9 for ^{15}N (Table 1).

We calculated a theoretical sensitivity gain for [^{15}N, ^{1}H]-TROSY-HNCA relative to conventional HNCA by using Eq. **8**,

$$\frac{A^T}{A^C} = \frac{R_2^C(^1\text{H}^N)}{2R_2^T(^1\text{H}^N)}\,exp[(R_2^C(^{15}\text{N}) - R_2^T(^{15}\text{N}))T], \qquad [8]$$

where A^T and A^C are the peak amplitudes in corresponding [^{15}N, ^{1}H]-TROSY-HNCA and conventional HNCA experiments, respectively. The amplitudes are linearly proportional to the ^{1}H^N relaxation rates, whereas the dependence on the ^{15}N transverse relaxation rates is exponential because of the ct evolution in the ^{15}N dimension (15). For a 23-kDa protein, Eq. **8** predicts an 8-fold sensitivity gain for the hypothetical isolated ^{15}N–^{1}H^N moiety. When allowing for DD coupling with remote protons, the gain for β-sheets and α-helices amounts to 4.7 and 2.9 in deuterated proteins and to 1.8 and 2.0 in protonated proteins, respectively. Sensitivity gains measured for the ^{2}H/^{13}C/^{15}N-labeled gyrase-23B were 3.4 for β-sheets and 2.9 for α-helices, and for ^{13}C/^{15}N-labeled FimC, a gain of 1.7 was measured for the β-sheet regions. These experimental data are in good agreement with the theoretical predictions (Table 1).

The sensitivity gain (Eq. **8**) depends on the molecular size. Fig. 5 shows the relative peak amplitudes calculated for [^{15}N, ^{1}H]-TROSY-HNCA (bold lines) and for conventional HNCA (thin lines) as a function of the rotational correlation time, using the parameters listed in Table 1. The thick and thin solid lines indicate the peak intensities for ^{15}N–^{1}H^N moieties located in β-sheet regions of a ^{2}H/^{13}C/^{15}N-labeled protein. The dashed lines show the corresponding intensities expected for a ^{13}C/^{15}N-labeled protein. The rapid decrease of the peak amplitude with increasing molecular size limits the application of the conventional HNCA experiment to much smaller proteins than [^{15}N, ^{1}H]-TROSY-HNCA (Fig. 5). Actually, for deuterated proteins similar peak

Table 1. Transverse ^{1}H^N and ^{15}N relaxation rates predicted for a 23-kDa protein at 750 MHz in [^{15}N, ^{1}H]-TROSY-HNCA and in conventional HNCA*

	TROSY-HNCA		HNCA		Gain[†]
	$R_2^T(^{15}$N)[s^{-1}]	$R_2^T(^1$H^N) [s^{-1}]	$R_2^C(^{15}$N) [s^{-1}]	$R_2^C(^1$H^N) [s^{-1}]	A^T/A^C
Isolated ^{15}N–^{1}H^N group	3.0	3.2	20.9	20.3	8.0
β-sheet ^{13}C/^{15}N-labeled[‡]	10.6	41.1	28.5	58.2	1.8
α-helix ^{13}C/^{15}N-labeled[§]	8.7	31.5	26.6	48.6	2.0
β-sheet ^{2}H/^{13}C/^{15}N-labeled[¶]	3.7	6.3	21.6	23.5	4.7
α-helix ^{2}H/^{13}C/^{15}N-labeled[‖]	5.0	13.2	22.9	30.3	2.9

*^{15}N and ^{1}H^N relaxation rates were calculated using Eqs. **6** and **7**, respectively, as described in the text. The values listed for conventional HNCA are the average relaxation rates of both components of the ^{15}N and the ^{1}H^N doublets, given by R_s^N and R_r^N, and by R_s^H and R_r^H, respectively. The following parameters were used: r_{HN} = 1.04 Å (39), $\Delta\sigma_N$ = 155 ppm, $\Delta\sigma_H$ = 15 ppm, Θ_N = 15°, Θ_H = 10° (40), and τ_c = 15 ns.

[†]A^T and A^C are the relative signal intensities obtained with [^{15}N, ^{1}H^N]-TROSY-HNCA and conventional HNCA. The ratio A^T/A^C was calculated with Eq. **8**, using T = 52 ms.

[‡]Remote protons considered are ^{1}H^N (i − 1), ^{1}H^N (i + 1), ^{1}H^N (j), ^{1}H$^\alpha$ (i), ^{1}H$^\alpha$ (i − 1), ^{1}H$^\alpha$ (j), ^{1}H$^\beta$ (i), and ^{1}H$^\beta$ (i − 1) at distances of 4.3, 4.3, 3.3, 2.8, 2.2, 3.2, 2.5, and 3.2 Å, respectively, which are typical for an antiparallel β-sheet [i is the observed residue, (i − 1) and (i + 1) the sequential neighbors, and j indicates a long-range contact across the β-sheet (2)].

[§]Remote protons are ^{1}H^N (i − 1), ^{1}H^N (i + 1), ^{1}H^N (i − 2), ^{1}H^N (i + 2), ^{1}H$^\alpha$ (i), ^{1}H$^\alpha$(i − 1), ^{1}H$^\alpha$(i − 2), ^{1}H$^\alpha$(i − 3), ^{1}H$^\alpha$(i − 4), and ^{1}H$^\beta$(i) at distances of 2.8, 2.8, 4.2, 4.2, 2.6, 3.5, 4.4, 3.4, 4.2, and 2.5 Å, respectively, which are typical for an α-helix (2).

[¶]Remote protons are ^{1}H^N (i − 1), ^{1}H^N (i + 1), and ^{1}H^N (j) at 4.3, 4.3, and 3.3 Å (2).

[‖]Remote protons are ^{1}H^N (i − 1), ^{1}H^N (i + 1), ^{1}H^N (i − 2), and ^{1}H^N (i + 2) at 2.8, 2.8, 4.2, and 4.2 Å (2).

FIG. 5. Relative signal amplitudes, A, calculated during the ct ^{15}N evolution and ^{1}H acquisition periods for [^{15}N, ^{1}H]-TROSY-HNCA (thick lines) and conventional HNCA (thin lines) at a magnetic field strength of 750 MHz for variable isotropic rotational correlation times, τ_c, in the range from 5 to 80 ns, which corresponds to protein sizes in H$_2$O solution at 20°C from $\approx$7 kDa at τ_c = 5 ns to $\approx$260 kDa at τ_c = 80 ns. The solid and dashed lines represent the signal amplitudes, A, for a ^{15}N–^{1}H^N moiety in a β-sheet of a deuterated and a protonated ^{13}C/^{15}N-labeled protein, respectively (see Table 1 for the parameters used). (*Inset*) An expanded plot for the range of A from 0 to 1. The dotted vertical line indicates the τ_c value of 15 ns estimated for the 23-kDa proteins gyrase-23B and FimC.

amplitudes are expected for τ_c = 15 ns with HNCA and τ_c = 50 ns with [^{15}N, ^{1}H]-TROSY-HNCA. For τ_c values above 15 ns, [^{15}N, ^{1}H]-TROSY-HNCA with protonated proteins is predicted to yield similar sensitivity as conventional HNCA with deuterated proteins (see Fig. 5).

Similar results to those obtained here with [^{15}N, ^{1}H]-TROSY-HNCA are predicted for the use of [^{15}N, ^{1}H]-TROSY with other triple-resonance experiments that use coherence pathways with ct ^{15}N evolution periods. For HNCO this is born out by the experiment in Fig. 4, and similar results have been obtained for HN(CO)CA (15), HNCACB (31, 32), and HN(CO)CACB (7,33) (M.S., G.W., K.P., H.S., and K.W., unpublished results). Overall, the present investigation predicts that TROSY-type triple-resonance experiments (Figs. 1 and 4) will be applicable for the assignment of significantly larger proteins than the corresponding conventional triple-resonance experiments. The predictions of Fig. 5 may serve as a platform for estimating the feasibility of resonance assignments and the instrument time needed for particular proteins in the size range 10–250 kDa. Thereby, one has to take into account that these curves can only provide a general guideline, since the CSA parameters may be somewhat variable in the individual amino acid residues (34–38).

Appendix

The transverse ^{15}N relaxation rate is calculated for a four-spin system *H-N-C-K* representing the backbone atoms ^{1}H^N, ^{15}N, and ^{13}C$^\alpha$ and a remote proton *K*, with scalar couplings $^1J_{HN}$, $^1J_{NC}$, and J_{KN}. ^{13}CO, which is not considered (see below), would be treated in the same way as ^{13}C$^\alpha$. The following single spin transition basis operators (47) were selected to evaluate the transverse relaxation of the ^{15}N single-quantum coherences that evolve in [^{15}N, ^{1}H]-TROSY-HNCA:

$$B^\pm = \begin{bmatrix} B_1^\pm \\ B_2^\pm \\ B_3^\pm \\ B_4^\pm \\ B_5^\pm \\ B_6^\pm \\ B_7^\pm \\ B_8^\pm \end{bmatrix} = \begin{bmatrix} N^\pm(1/2 + H_z)(1/2 + K_z)(1/2 + C_z) \\ N^\pm(1/2 - H_z)(1/2 + K_z)(1/2 + C_z) \\ N^\pm(1/2 + H_z)(1/2 + K_z)(1/2 - C_z) \\ N^\pm(1/2 - H_z)(1/2 + K_z)(1/2 - C_z) \\ N^\pm(1/2 + H_z)(1/2 - K_z)(1/2 + C_z) \\ N^\pm(1/2 - H_z)(1/2 - K_z)(1/2 + C_z) \\ N^\pm(1/2 + H_z)(1/2 - K_z)(1/2 - C_z) \\ N^\pm(1/2 - H_z)(1/2 - K_z)(1/2 - C_z) \end{bmatrix}. \quad \textbf{[A1]}$$

In this basis, the Liouville matrix in the rotating frame has the diagonal form given by Eq. **A2**:

$$L = \begin{bmatrix} \omega_r^N + \pi^1J_{NC} + \pi J_{NK} & & & & \\ & \omega_s^N + \pi^1J_{NC} + \pi J_{NK} & & & 0 \\ & & \omega_r^N - \pi^1J_{NC} + \pi J_{NK} & & \\ & & & \omega_s^N - \pi^1J_{NC} + \pi J_{NK} & \\ & & & & \omega_r^N + \pi^1J_{NC} - \pi J_{NK} \\ & & & & \quad \omega_s^N + \pi^1J_{NC} - \pi J_{NK} \\ 0 & & & & \qquad \omega_r^N - \pi^1J_{NC} - \pi J_{NK} \\ & & & & \qquad \quad \omega_s^N - \pi^1J_{NC} - \pi J_{NK} \end{bmatrix}, \quad \textbf{[A2]}$$

with $\omega_r^N = \Omega^N - \Omega_0 + \pi^1J_{HN}$ and $\omega_s^N = \Omega^N - \Omega_0 - \pi^1J_{HN}$, where Ω_0 is the reference frequency and Ω^N the Larmor frequency of *N*. In calculating the relaxation matrix, Γ, the DD interactions *H-N*, *N-C*, *C-K*, and *H-K*, the CSA of *H* and *N*, and all cross-correlation terms between these relaxation interactions are taken into account. Not included are the very small *N-C* DD interactions (48). In the slow-tumbling approximation, only terms in $J(0)$ need to be retained:

$$\Gamma = \begin{bmatrix} \Gamma_{11} & 0 & 0 & 0 & 0 & 0 & 0 & 0 \\ 0 & \Gamma_{22} & 0 & 0 & \Gamma_{25} & 0 & 0 & 0 \\ 0 & 0 & \Gamma_{33} & 0 & 0 & 0 & 0 & 0 \\ 0 & 0 & 0 & \Gamma_{44} & 0 & 0 & \Gamma_{47} & 0 \\ 0 & \Gamma_{52} & 0 & 0 & \Gamma_{55} & 0 & 0 & 0 \\ 0 & 0 & 0 & 0 & 0 & \Gamma_{66} & 0 & 0 \\ 0 & 0 & 0 & \Gamma_{74} & 0 & 0 & \Gamma_{77} & 0 \\ 0 & 0 & 0 & 0 & 0 & 0 & 0 & \Gamma_{88} \end{bmatrix}, \quad \textbf{[A3]}$$

where the Γ_{ii} represent the relaxation rates of individual transitions of the *N* multiplet. Γ_{25}, Γ_{52}, Γ_{47}, and Γ_{74} represent the cross-relaxation between different nondegenerate transitions of the *N* multiplet with resonance frequencies separated by π^1J_{HN}. The individual relevant matrix elements are:

$$\Gamma_{11} = (p_{HN}^2 + 2f_{p_{HN}\delta_N}p_{HN}\delta_N + \delta_N^2 + p_{CN}^2 + 2f_{p_{CN}\delta_N}p_{CN}\delta_N$$
$$+ 2f_{p_{CN}p_{HN}}p_{CN}p_{HN}) \cdot 4J(0) \quad \textbf{[A4]}$$

$$\Gamma_{22} = (p_{HN}^2 - 2f_{p_{HN}\delta_N}p_{HN}\delta_N + \delta_N^2 + p_{CN}^2 + 2f_{p_{CN}\delta_N}p_{CN}\delta_N$$
$$- 2f_{p_{CN}p_{HN}}p_{CN}p_{HN} + 0.5p_{HK}^2) \cdot 4J(0) \quad \textbf{[A5]}$$

$$\Gamma_{33} = p_{HN}^2 + 2f_{p_{HN}\delta_N}p_{HN}\delta_N + \delta_N^2 + p_{CN}^2 - 2f_{p_{CN}\delta_N}p_{CN}\delta_N$$
$$- 2f_{p_{CN}p_{HN}}p_{CN}p_{HN}) \cdot 4J(0) \quad \textbf{[A6]}$$

$$\Gamma_{44} = p_{HN}^2 - 2f_{p_{HN}\delta_N}p_{HN}\delta_N + \delta_N^2 + p_{CN}^2 - 2f_{p_{CN}\delta_N}p_{CN}\delta_N$$
$$+ 2f_{p_{CN}p_{HN}}p_{CN}p_{HN} + 0.5p_{HK}^2) \cdot 4J(0) \quad \textbf{[A7]}$$

$$\Gamma_{44} = p_{HN}^2 + 2f_{p_{HN}\delta_N}p_{HN}\delta_N + \delta_N^2 + p_{CN}^2 + 2f_{p_{CN}\delta_N}p_{CN}\delta_N$$
$$+ 2f_{p_{CN}p_{HN}}p_{CN}p_{HN} + 0.5p_{HK}^2) \cdot 4J(0) \quad \textbf{[A8]}$$

$$\Gamma_{66} = p_{HN}^2 - 2f_{p_{HN}\delta_N}p_{HN}\delta_N + \delta_N^2 + p_{CN}^2 + 2f_{p_{CN}\delta_N}p_{CN}\delta_N$$
$$- 2f_{p_{CN}p_{HN}}p_{CN}p_{HN}) \cdot 4J(0) \quad \textbf{[A9]}$$

$$\Gamma_{77} = p_{HN}^2 + 2f_{p_{HN}\delta_N}p_{HN}\delta_N + \delta_N^2 + p_{CN}^2 - 2f_{p_{CN}\delta_N}p_{CN}\delta_N$$
$$- 2f_{p_{CN}p_{HN}}p_{CN}p_{HN} + 0.5p_{HK}^2) \cdot 4J(0) \quad \textbf{[A10]}$$

$$\Gamma_{66} = p_{HN}^2 - 2f_{p_{HN}\delta_N}p_{HN}\delta_N + \delta_N^2 + p_{CN}^2 - 2f_{p_{CN}\delta_N}p_{CN}\delta_N$$
$$+ 2f_{p_{CN}p_{HN}}p_{CN}p_{HN}) \cdot 4J(0) \quad \textbf{[A11]}$$

$$\Gamma_{25} = \Gamma_{52} = \Gamma_{47} = \Gamma_{74} = -p_{HK}^2 \cdot 2J(0) \quad \textbf{[A12]}$$

$f_{ki} = 0.5(3\cos^2\Theta_{kl} - 1)$, $p_{ij} = (2\sqrt{2}r_{ij}^3)^{-1}\hbar\gamma_i\gamma_j$ and $\delta_N = (3\sqrt{2})^{-1}\gamma_N B_0 \Delta\sigma_N$, where $\hbar$ is the Planck constant divided by 2π, Θ_{kl} the angle between the unique tensor axes of the interactions k and l, γ_i the gyromagnetic ratio of spin i, r_{ij} the distance between the spins i and j, B_0 the polarizing magnetic field, and $\Delta\sigma_N$ the difference between the axial and perpendicular principal components of the ^{15}N chemical shift tensor, which is assumed to be axially symmetric. Numerical calculations using Eqs. **A4–A12** showed that the terms ($p_{CN}^2 \pm 2f_{p_{CN}\delta_N} p_{CN}\delta_N \pm 2f_{p_{CN}p_{HN}} p_{CN}p_{HN})\cdot 4J(0)$ contribute <10% to the overall relaxation of ^{15}N and can be neglected. This applies for both ^{13}C$^\alpha$ and ^{13}CO. The Eqs. **A2** and **A3** show that there is no interference between the group of basis operators $B_1^\pm$, $B_3^\pm$, $B_6^\pm$, and $B_8^\pm$ and the other four basis operators. Thus, for these operators, the time evolution can be calculated individually, resulting in single-exponential relaxation determined exclusively by interactions within the *H-N* spin subsystem. Because of the pairwise linkage of $B_2^\pm$ with $B_5^\pm$, and of $B_4^\pm$ with $B_7^\pm$, the relaxation of the corresponding transitions is in general biexponential. However, since $\Gamma_{ij} \ll \pi^1 J_{HN}$ ($i \neq j$) the off-diagonal elements can be neglected, so that a single-exponential decay is obtained for all basis operators:

$$\langle B_i^\pm\rangle(t) = \langle B_i^\pm\rangle(0)\cdot exp[\mp(iL_{ii} + \Gamma_{ii})t](i = 1 \ldots 8). \quad \textbf{[A13]}$$

The sum of the operators $B_2^\pm$, $B_4^\pm$, $B_6^\pm$, and $B_8^\pm$ represents the magnetization of the TROSY ^{15}N multiplet component, so that the transverse ^{15}N magnetization at time t can be described by:

$$\langle B_2^\pm + B_4^\pm + B_6^\pm + B_8^\pm\rangle(t)$$

$$= N_s^\pm(cos[\pi^1 J_{NC}t] \mp 2iC_z sin[\pi^1 J_{NC}t])\cdot exp[\mp i\omega_s^N t]$$

$$\cdot exp[-R_s^N t]\cdot 0.5\{exp[i\pi J_{NK}] + exp[-i\pi J_{NK} - p_{HK}^2\cdot 2J(0)]$$

$$\mp K_z(exp[i\pi J_{NK}] - exp[-i\pi J_{NK} - p_{HK}^2\cdot 2J(0)])\}, \quad \textbf{[A14]}$$

where $N_s^\pm = N^\pm(1/2 - H_z)$ and $R_s^N = (p_{HN}^2 - 2f_{p_{HN}\delta_N} p_{HN}\delta_N + \delta_N^2)\cdot 4J(0)$. Eq. **A14** can be further simplified by assuming that $J_{NK} = 0$. Furthermore, since $N^\pm K_z$ does not result in an observable signal, the evolution of the ^{15}N magnetization can be described by **A15**:

$$\langle N_s^\pm\rangle(t) = \langle N_s^\pm\rangle(0)\{cos[\pi^1 J_{NC}t] \mp 2iC_z sin[\pi^1 J_{NC}t]\}$$

$$\cdot exp[\mp i\omega_s^N t]\cdot exp[-R_s^N t]\cdot 0.5(1 + exp[-2p_{HK}^2 J(0)t]).$$

$$\textbf{[A15]}$$

This treatment can be expanded to n mutually noninteracting remote protons, $K^1, K^2, \ldots, K^n$, resulting in Eq. **A16**:

$$\langle N_s^\pm\rangle(t) = \langle N_s^\pm\rangle(0)\{cos[\pi^1 J_{NC}t] \mp 2iC_z sin[\pi^1 J_{NC}t]\}$$

$$\cdot exp[\mp i\omega_s^N t]\cdot exp[-R_s^N t]\cdot \prod_{j=1}^{n} 0.5(1 + exp[-2p_{HK^j}^2 J(0)t],$$

$$\textbf{[A16]}$$

Eq. **A16** was used for the derivation of Eq. **3** in the main text.

1. Wüthrich, K., Wider, G., Wagner, G. & Braun, W. (1982) *J. Mol. Biol.* **155**, 311–319.
2. Wüthrich, K. (1986) *NMR of Proteins and Nucleic Acids* (Wiley, New York).
3. Montelione, G. T. & Wagner, G. (1989) *J. Am. Chem. Soc.* **111**, 5474–5475.
4. Ikura, M., Kay, L. E. & Bax, A. (1990) *Biochemistry* **29**, 4659–4667.
5. Bax, A. & Grzesiek, S. (1993) *Acc. Chem. Res.* **26**, 131–138.
6. Edison, A. S., Abildgaard, F., Westler, W. M., Mooberry, E. S. & Markley, J. (1994) *Methods Enzymol.* **239**, 3–79.
7. Yamazaki, T., Lee, W., Arrowsmith, C. H., Muhandiram, D. R. & Kay, L. E. (1994) *J. Am. Chem. Soc.* **116**, 11655–11666.
8. LeMaster, D. M. (1994) *Prog. Nucl. Magn. Reson. Spectrosc.* **26**, 371–419.
9. Kay, L. E. & Gardner, K. H. (1997) *Curr. Opin. Struct. Biol.* **7**, 722–731.
10. Pervushin, K., Riek, R., Wider, G. & Wüthrich, K. (1997) *Proc. Natl. Acad. Sci. USA* **94**, 12366–12371.
11. Kay, L. E., Ikura, M., Tschudin, R. & Bax, A. (1990) *J. Magn. Reson.* **89**, 496–514.
12. Grzesiek, S. & Bax, A. (1992) *J. Magn. Reson.* **96**, 432–440.
13. Yamazaki, T., Lee, W., Revington, M., Mattiello, D. L., Dahlquist, F. W., Arrowsmith, C. H. & Kay, L. E. (1994) *J. Am. Chem. Soc.* **116**, 6464–6465.
14. Vuister, G. W. & Bax, A. (1992) *J. Magn. Reson.* **98**, 428–435.
15. Wider, G. (1998) *Prog. Nucl. Magn. Reson. Spectrosc.* **32**, 193–275.
16. Sørensen, O. W., Eich, G. W., Levitt, M. H., Bodenhausen, G. & Ernst, R. R. (1983) *Prog. Nucl. Magn. Reson. Spectrosc.* **16**, 163–192.
17. Ernst, R. R., Bodenhausen, G. & Wokaun, A. (1987) *The Principles of Nuclear Mangetic Resonance in One and Two Dimensions* (Clarendon, Oxford), pp. 38–40.
18. Pervushin, K., Wider, G. & Wüthrich, K. (1998) *J. Biomol. Nucl. Magn. Reson.* **12**, 345–348.
19. Pervushin, K., Riek, R., Wider, G. & Wüthrich, K. (1998) *J. Am. Chem. Soc.* **120**, 6394–6400.
20. Farrar, T. C. & Stringfellow, T. C. (1996) in *Encyclopedia of NMR*, eds. Grant, D. M. & Harris, R. K. (Wiley, New York), Vol. 6, pp. 4101–4107.
21. Szyperski, T., Braun, D., Fernandez, C., Bartels, C. & Wüthrich, K. (1995) *J. Magn. Reson. B* **108**, 197–203.
22. Lewis, R. J., Singh, O. M., Smith, C. V., Skarzynski, T., Maxwell, A., Wonacott, A. J. & Wigley, D. B. (1996) *EMBO J.* **15**, 1412–1420.
23. Wigley, D. B. (1995) *Annu. Rev. Biophys. Biomol. Struct.* **24**, 185–208.
24. Maxwell, A. (1997) *Trends Microbiol.* **5**, 102–109.
25. Pellecchia, M., Güntert, P., Glockshuber, R. & Wüthrich, K. (1998) *J. Biomol. Nucl. Magn. Reson.* **11**, 229–230.
26. DeMarco, A. & Wüthrich, K. (1976) *J. Magn. Reson.* **24**, 201–204.
27. Güntert, P., Dötsch, V., Wider, G. & Wüthrich, K. (1992) *J. Biomol. Nucl. Magn. Reson.* **2**, 619–629.
28. Bartels, C., Xia, T., Billeter, M., Güntert, P. & Wüthrich, K. (1995) *J. Biomol. Nucl. Magn. Reson.* **5**, 1–10.
29. Kay, L. E., Torchia, D. A. & Bax, A. (1989) *Biochemistry* **28**, 8972–8979.
30. Muhandiram, D. R. & Kay, L. E. (1994) *J. Magn. Reson. B* **103**, 203–216.
31. Grzesiek, S. & Bax, A. (1992) *J. Magn. Reson.* **99**, 201–207.
32. Wittekind, M. & Mueller, L. (1993) *J. Magn. Reson. B* **101**, 201–205.
33. Grzesiek, S. & Bax, A. (1992) *J. Am. Chem. Soc.* **114**, 6291–6292.
34. Tjandra, N. & Bax, A. (1997) *J. Am. Chem. Soc.* **119**, 8076–8082.
35. Tessari, M., Mulder, F. A. A., Boelens, R. & Vuister, G. W. (1997) *J. Magn. Reson.* **127**, 128–133.
36. Tessari, M., Vis, H., Boelens, R., Kaptein, R. & Vuister, G. W. (1997) *J. Am. Chem. Soc.* **119**, 8985–8990.
37. Fushman, D. & Cowburn, D. (1998) *J. Am. Chem. Soc.* **120**, 7109–7110.
38. Fushman, D., Tjandra, N. & Cowburn, D. (1998) *J. Am. Chem. Soc.*, in press.
39. Roberts, J. E., Harbison, G. S., Munowitz, M. G., Herzfeld, J. & Griffin, R. G. (1987) *J. Am. Chem. Soc.* **109**, 4163–4169.
40. Wu, C. H., Ramamoorthy, A., Gierasch, L. M. & Opella, S. J. (1995) *J. Am. Chem. Soc.* **117**, 6148–6149.
41. Kay, L. E., Keifer, P. & Saarinen, T. (1992) *J. Am. Chem. Soc.* **114**, 10663–10664.
42. Marion, D., Ikura, M., Tschudin, R. & Bax, A. (1989) *J. Magn. Reson.* **85**, 393–399.
43. Grzesiek, S. & Bax, A. (1993) *J. Am. Chem. Soc.* **115**, 12593–12594.
44. Piotto, M., Saudek, V. & Sklenar, V. J. (1992) *J. Biomol. Nucl. Magn. Reson.* **2**, 661–665.
45. Shaka, A. J., Keeler, J., Frenkiel, T. & Freeman, R. (1983) *J. Magn. Reson.* **52**, 335–338.
46. Cavanagh, J. & Rance, M. (1992) *J. Magn. Reson.* **96**, 670–678.
47. Vold, R. R. & Vold, R. R. (1976) *J. Chem. Phys.* **64**, 320–324.
48. Peng, J. W. & Wagner, G. (1992) *J. Magn. Reson.* **98**, 308–332.